

SUPPORTING INFORMATION

Interplay Between Dopant Species and a Spin-Crossover Host Lattice during Light-Induced Excited Spin-State Trapping Probed by EPR Spectroscopy

Sergey V. Tumanov^{ab}, Sergey L. Veber^{ab}, Sam Greatorex^c, Malcolm A. Halcrow^{*c}
and Matvey V. Fedin^{*ab}

^a International Tomography Center SB RAS, Institutskaya str. 3a, 630090 Novosibirsk, Russia.
E-mail: mfedin@tomo.nsc.ru

^b Novosibirsk State University, Pirogova str.2, 630090 Novosibirsk, Russia.

^c School of Chemistry, University of Leeds, Leeds LS2 9JT, UK.
E-mail: m.a.halcrow@leeds.ac.uk

	Page
Figure S1 The LIESST effect in undoped [Fe(bpp) ₂][BF ₄] ₂ and compound 1 .	S2
1. Details of the EPR spectroscopy for 1.	S3
Figure S2. Q-band CW EPR spectra of 1 at 20 K, before and after irradiation.	S3
2. Details of the EPR spectroscopy for 2.	S5
Figure S3. Simulations of the Q-band EPR spectra of 2 shown in Fig. 2 of the main text; and, EPR spectra of 2 at 20 K, before and after irradiation.	S5
Figure S4. Experimental and simulated Q-band EPR spectra of 2 vs. temperature recorded without illumination.	S5
3. Details of the EPR spectroscopy for 3.	S6
Figure S5. Simulations of the Q-band EPR spectra of 3 shown in Fig. 3 of the main text; and, EPR spectra of 2 at 20 K, before and after irradiation.	S6
Figure S6. Experimental and simulated Q-band EPR spectra of 3 vs. temperature recorded without illumination.	S6
4. Effects of sample preparation.	S7
Figure S7. Comparison of Q-band EPR spectra of 3 measured without illumination, as a KBr pellet and pure polycrystalline powder.	S7
5. Tabulated simulation parameters for 1-3.	S8
6. Description of the experimental EPR setup	S9
7. References	S10
	S1

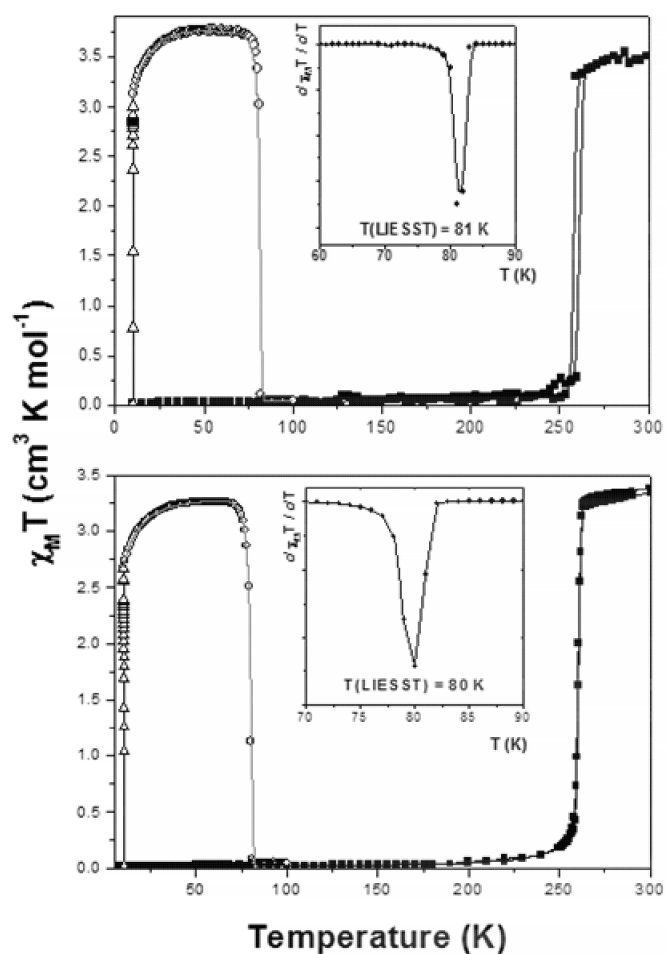


Fig. S1 The LIESST effect in undoped $[\text{Fe}(\text{bpp})_2][\text{BF}_4]_2$ (top) and compound **1** (bottom), from magnetic susceptibility measurements. ■ = data recorded in cooling and warming modes without irradiation; Δ = data recorded with irradiation at 10 K; \circ = data recorded in warming mode in the dark after irradiation for one hour. The insets show the derivate of the $d\chi_M T/dT$ vs. T curves, whose minimum corresponds to the $T(\text{LIESST})$ value. The Figure is adapted from ref 1 (copyright the Royal Society of Chemistry).

Comparable data from **2** and **3** have not been reported, but precedent suggests $T(\text{LIESST}) = 80 \pm 1$ K is to be expected for those compounds (which would also be consistent with the EPR data in this study).^{S1,S2}

1. Details of the EPR spectroscopy for **1**

Figure S2a compares the EPR spectrum of **1** at 20 K measured prior to illumination with the spectrum of “relaxed” compound at 20 K. The spectrum of “relaxed” compound refers to the measurement after a series of experiments including illumination, warming up to 90 K with the light switched off and cooling back again to 20 K. Within experimental accuracy, the spectra agree very well, supporting the complete reversibility of LIESST-relaxation cycles in **1**. Note that the absolute amount of cobalt(II) centers is rather small, because it corresponds only to 3% of all SCO centers, and at the same time the concentration of the whole mixed-metal compound cannot be very high to ensure a sufficient transparency of the KBr pellet for incident light. Therefore, the Co^{2+} signal is rather weak. In addition, since it is difficult to avoid microwave saturation completely, the spectral lineshape at 20 K is slightly distorted. Note, however, that for practical purposes and for determining the positions of resonance lines such minor imperfections are negligible.

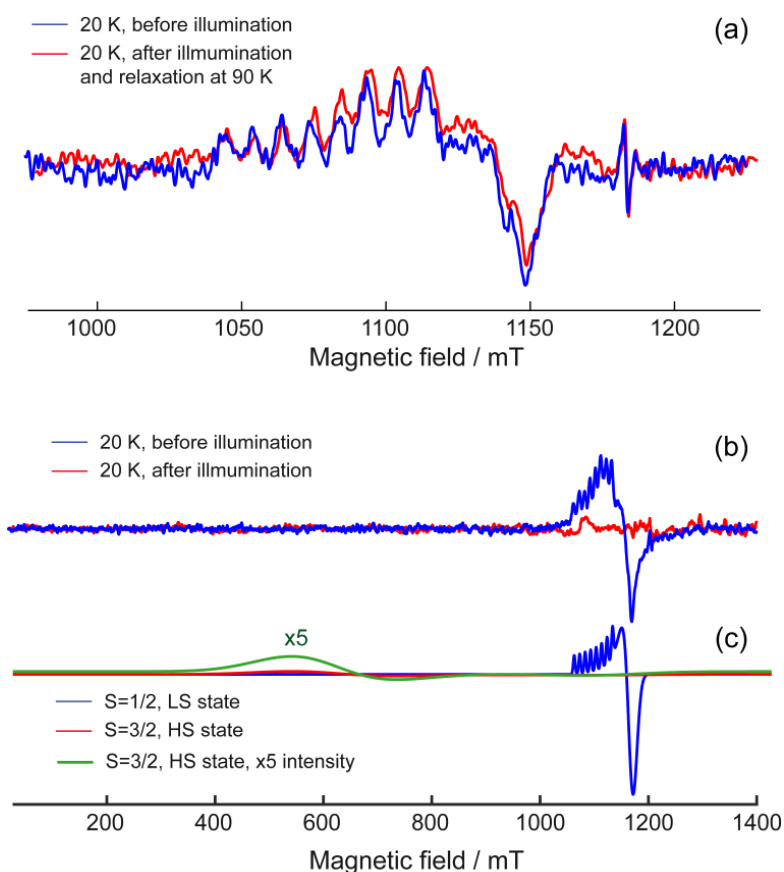


Fig. S2. (a) Q-band EPR spectra of **1** at 20 K: (blue) taken before illumination; (red) taken after illumination and series of experiments shown in Fig.1 of the main text (i.e., illumination, warming up to 90 K in the dark and cooling back to 20 K). (b) Q-band EPR spectra of **1** at 20 K measured in a broad range of magnetic field: (blue) taken before illumination; (red) taken immediately after illumination. (c) Simulations of Q-band spectra of LS ($S = 1/2$, blue) and HS ($S = 3/2$, red) spectra using the same set of parameters (given below in Table 5.1). For HS state $D \gg h\nu$ and linewidth of 100 mT were used. The green trace repeats the red one with magnified intensity by a factor of 5.

Figure S2b shows the EPR spectra of **1** measured in a broad range of magnetic field in the dark and upon irradiation with light. In principle, one would expect that the conversion of Co(II) from a low-spin ($S = 1/2$) to high-spin ($S = 3/2$) state must not only cause disappearance of the $S = 1/2$ spectrum at central field, but should also result in simultaneous appearance of the $S = 3/2$ spectrum. For typically large zero-field splittings (larger than the microwave quantum) such $S = 3/2$ features appear most clearly near effective $g \sim 4$ (for g_{\perp}). However, in our experiments no signature of the $S = 3/2$ spectrum was observed. This is unsurprising, because the intensity of LS $S = 1/2$ spectrum is already quite weak due to a presence of only $\sim 3\%$ of Co(II) in the compound and additional ‘dilution’ by dispersing it in a KBr disk (see above).

The intensity of the HS $S = 3/2$ spectrum must be much weaker compared to that of LS state, because the EPR spectrum of HS state is drastically broader for the same number of spins; and, electron relaxation of high-spin states is typically much faster. Figure S2c shows simulations illustrating the different intensities of the low-spin and high-spin EPR spectra. The same set of parameters was used in both cases (the parameters for the low-spin state are given below in Table 5.1). In addition, for the high-spin spectrum $D \gg h\nu$ and a linewidth of 100 mT were used. Such a broad linewidth is very realistic for high-spin Co(II) and even might be underestimated. For example, a linewidth of ~ 400 mT was experimentally observed for high-spin Co(II) in Fig. S15 of ref. S3.

This fully justifies the fact that the spectrum of the high-spin $S = 3/2$ state could not be detected. Nevertheless, the reversible disappearance of low-spin spectrum upon irradiation and its reappearance following the heating-cooling cycle has no other plausible explanation except for reversible spin-state conversion of the $[\text{Co}(\text{terpy})_2]^{2+}$ dopant.

2. Details of the EPR spectroscopy for **2**

Figure S3a reports simulations of all spectra shown in Fig. 2 of the main text, and Figure S3b confirms the reversibility of LIESST-relaxation cycles for **2**. Figure S4 shows the experimental and simulated spectra acquired without illumination. For similar reasons to those discussed previously for **1**, the lineshapes of experimental spectra are slightly distorted in the g_{\perp} region, which is however negligible for the purposes of this study.

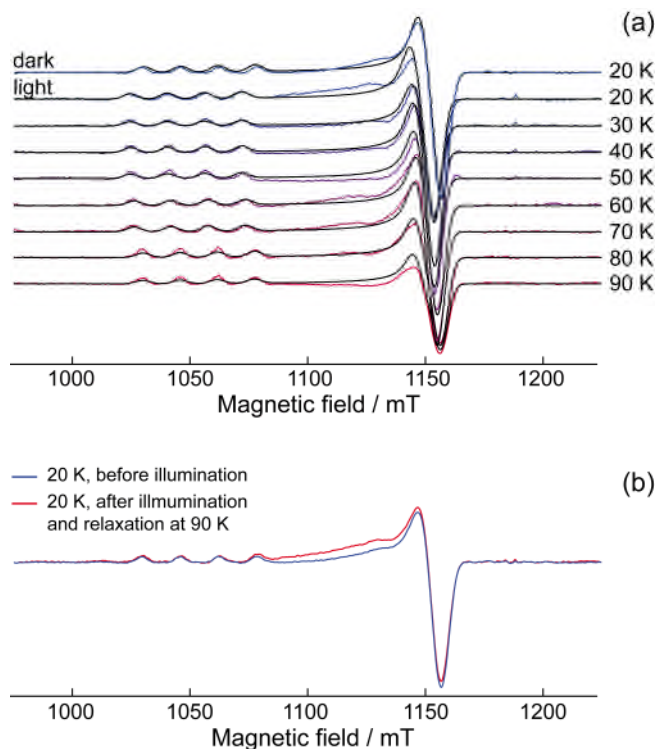


Fig. S3. (a) Simulations of the Q-band EPR spectra of **2** shown in Fig. 2 of the main text. Colored lines show the experimental data, black lines correspond to the best fits. Temperatures are indicated. (b) Comparison of spectra at 20 K: (blue) taken before illumination; (red) taken after illumination and series of experiments shown in Fig. 2 of the main article (i.e., illumination, warming to 90 K in the dark and recooling to 20 K).

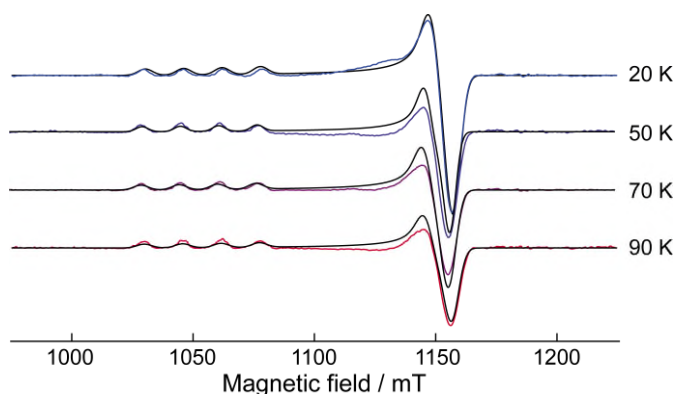


Fig. S4. Simulation of Q-band EPR spectra of **2** vs. temperature without illumination (this is the source of the g -values shown as insets in Fig. 2 of the main article). Colored lines show the experimental data, black lines correspond to the best fits. Temperatures are indicated.

3. Details of the EPR spectroscopy for **3**

Figure S5a reports simulations of all spectra shown in Fig. 3 of the main text, and Figure S5b confirms the reversibility of LIESST-relaxation cycles for **3**. Figure S6 shows the experimental and simulated spectra taken without illumination.

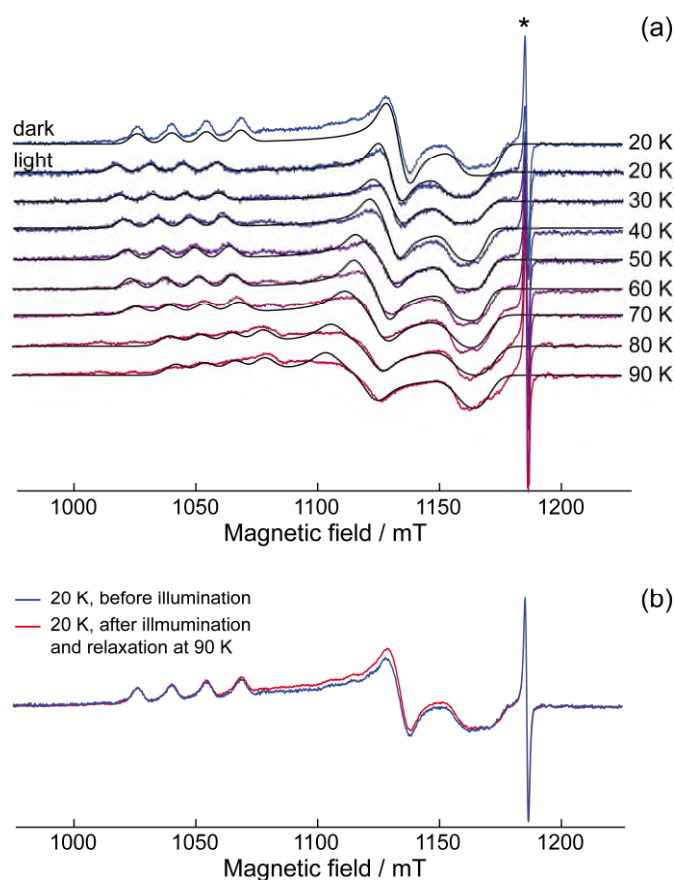


Fig. S5. (a) Simulation of Q-band EPR spectra of **3** shown in Fig. 3 of the main text. Colored lines show the experimental data, black lines correspond to the best fits. Asterisk marks radical impurity. Temperatures are indicated. (b) Comparison of spectra at 20 K: (blue) taken before illumination; (red) taken after illumination and series of experiments shown in Fig. 3 of the main article (i.e., illumination, warming to 90 K in the dark and recooling to 20 K).

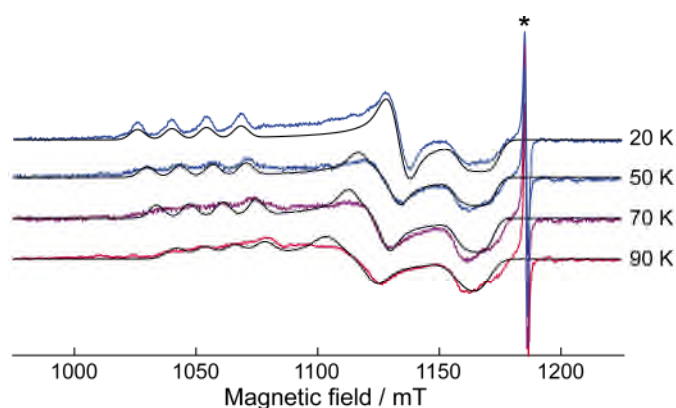


Fig. S6. Simulation of Q-band EPR spectra of **3** vs. temperature without illumination (this is the source of the g -values shown as insets in Fig. 3 of the main article). Colored lines show the experimental data, black lines correspond to the best fits. The asterisk marks a radical impurity and temperatures are indicated.

4. Effects of Sample Preparation

Using **3** as an example, Figure S7 illustrates the effect of sample preparation (compression of polycrystalline powder into a KBr pellet) on SCO properties of the host lattice. One obvious influence is the generation of radical center (marked by asterisk), which has a narrow EPR signal at $g \sim 2$ but does not disturb our experiments. The amount of generated impurity radical varies from sample to sample, and it also has a finite lifetime; the impurity signal is stronger for freshly prepared samples, and often decreases to almost zero after keeping the sample in a fridge for a few weeks. With respect to the target compound, the Cu^{2+} -derived signals in the $g_{x,y}$ region are very similar for both KBr pellet and polycrystalline powder. The most informative signals in the g_z region are also very similar between $T = 20\text{-}50\text{ K}$. However, they slightly differ from each other at temperatures close to $T(\text{LIESST})$, between $70\text{-}90\text{ K}$. We believe that this indicates that the SCO becomes less abrupt (more gradual) in the pellet due to the exposure to an external pressure, resulting in a broadening of the four g_z peaks at $\sim 70\text{-}90\text{ K}$. Such phenomena are known, and, for instance, have been recently observed by us for the other SCO-like materials.^{S4}

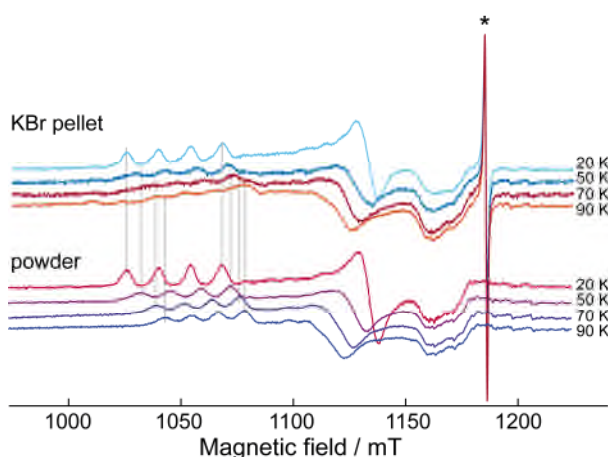


Fig. S7. Variable-temperature Q-band EPR spectra of **3** measured without illumination using KBr pellet (top) and pure polycrystalline powder (bottom). Temperatures are indicated. Asterisk marks radical impurity. Grey vertical lines guide the eye for comparison of the corresponding line positions.

5. Simulation parameters for 1-3

All simulations in the main text and SI used the following sets of parameters, where $g_{x,y,z}$ are the principal components of the g -tensor ($g_{\perp} = g_{x,y}$ and $g_{\parallel} = g_z$ for axial symmetry); $A_{xx,yy,zz}$ are the principal components of the hyperfine interaction tensor ($A_{\perp} = A_{xx,yy}$ and $A_{\parallel} = A_{zz}$ for axial symmetry); and ν_{mw} is the microwave frequency. The error on the simulated g -values is $ca \pm 0.002$.

EPR parameters in frozen solution for the dopant complexes in **2** and **3** are also provided, for comparison. No frozen solution data are available for the low-spin form of the $[\text{Co}(\text{terpy})_2]^{2+}$ dopant in **1**.

5.1. Compound 1

Compound	1	
	dark	irradiated
T / K	20	90
g_x	2.060	2.068
g_y	2.100	2.088
g_z	2.200	2.201
$A_{xx,yy} / \text{MHz}$	$\sim 110^*$	$\sim 50^*$
A_{zz} / MHz	300	310
ν_{mw} / GHz	≈ 33.11	

* These values are rough estimates, since $A_{xx,yy}$ is poorly resolved.

5.2. Compound 2

Compound	2											$[\text{Cu}(\text{terpy})_2][\text{PF}_6]_2^{\text{S5}}$
	dark			irradiated								relaxed
T / K	20	50	70	30	40	50	60	70	80	90	20	15
g_{\perp}	2.061	2.062	2.063	2.066	2.066	2.065	2.063	2.064	2.063	2.063	2.060	2.062
g_{\parallel}	2.252	2.256	2.257	2.268	2.267	2.268	2.264	2.264	2.256	2.256	2.255	2.260
A_{\perp} / MHz	61	70	70	54	56	49	53	56	74	76	70	58
$A_{\parallel} / \text{MHz}$	500											500
ν_{mw} / GHz	≈ 33.27											

5.3. Compound 3

Compound	3											$[\text{Cu}(\text{bpp})_2][\text{BF}_4]_2^{\text{S6}}$
	dark			irradiated								relaxed
T / K	20	50	70	30	40	50	60	70	80	90	20	120
g_x	2.038	2.042	2.042	2.049	2.047	2.047	2.047	2.045	2.042	2.043	2.037	2.051
g_y	2.099	2.113	2.121	2.107	2.109	2.115	2.119	2.124	2.131	2.135	2.099	2.099
g_z	2.270	2.264	2.256	2.288	2.284	2.280	2.277	2.272	2.246	2.243	2.270	2.281
A_{xx} / MHz	120	120	120	120	100	120	110	110	120	100	120	–
A_{yy} / MHz	50	120	120	80	80	120	100	120	150	150	50	–
A_{zz} / MHz	450	430	430	430	430	430	430	430	400	380	450	437
ν_{mw} / GHz	$\approx 33.27 \text{ GHz}$											

6. Description of the experimental EPR setup

All measurements were carried out using a commercial Bruker Elexsys E580 EPR spectrometer at Q-band in continuous wave mode. The spectrometer was equipped with Oxford Instruments temperature control system ER 4112HV-F including continuous gas flow cryostat, pumps and all accessories. In all experiments we used Q-band resonator ER 5106 QT-W. Photoillumination was performed with a 532 nm OLED fed directly into the EPR probe by an optical fiber. The fiber was inserted directly into EPR sample tube from the top, through the sample holder, and illuminated from outside the cryostat. A small piece of a KBr pellet with target compound dispersed in it was placed on the bottom of 1.8 mm ID / 2.8 mm OD quartz tube with the plane perpendicular to the fiber direction. In such conditions maximum photoswitching efficiency was obtained.

The spectra were recorded using standard experimental settings with modulation amplitude being 3-10 Gs and microwave power adjusted as a trade-off between signal intensity, baseline stability and nearly absent saturation. Number of scans varied depending on temperature and sample amount.

7. References

- (S1) Chastanet, G.; Tovee, C. A.; Hyett, G.; Halcrow, M. A.; Létard, J.-F. Photomagnetic Studies on Spin-Crossover Solid Solutions Containing Two Different Metal Complexes, $[\text{Fe}(\text{1-bpp})_2]_x[\text{M}(\text{terpy})_2]_{1-x}[\text{BF}_4]_2$ ($\text{M} = \text{Ru}$ or Co). *Dalton Trans.* **2012**, *41*, 4896–4902.
- (S2) Halcrow, M. A.; Chastanet, G. Spin-crossover and the LIESST Effect in $[\text{Fe}_x\text{Co}_{1-x}(\text{bpp})_2][\text{BF}_4]_2$ ($1.00 \geq x \geq 0.77$). Comparison with Bifunctional Solid Solutions of Iron and Cobalt Spin-Crossover Centers. *Polyhedron* **2017**, *136*, 5–12.
- (S3) Voloshin, Ya. Z., Varzatskii, O. A.; Novikov, V. V.; Strizhakova, N. G.; Vorontsov, I. I.; Vologzhanina, A. V.; Lyssenko, K. A.; Romanenko, G. V.; Fedin, M. V.; Ovcharenko, V. I.; Bubnov, Yu. N. *Tris*-Dioximate Cobalt(I,II,III) Clathrochelates: Stabilization of Different Oxidation and Spin States of an Encapsulated Metal Ion by Ribbed Functionalization. *Eur. J. Inorg. Chem.* **2010**, 5401–5415.
- (S4) Veber, S. L.; Sutura, E. A.; Fedin, M. V.; Boldyrev, K. N.; Maryunina, K. Y.; Sagdeev, R. Z.; Ovcharenko, V. I.; Gritsan, N. P.; Bagryanskaya, E. G. FTIR Study of Thermally Induced Magnetostructural Transitions in Breathing Crystals. *Inorg. Chem.* **2015**, *54*, 3446–3455.
- (S5) Narr, E.; Zimmermann, H.; Godt, A.; Goldfarb, D.; Jeschke, G. Structure and Dynamics of Copper Complexes with 2,2':6',2''-Terpyridines in Glassy Matrices. *Phys. Chem. Chem. Phys.* **2003**, *5*, 3959–3967.
- (S6) Solanki, N. K.; McInnes, E. J. L.; Mabbs, F. E.; Radojevic, S.; McPartlin, M.; Feeder, N.; Davies, J. E.; Halcrow, M. A. Steric Control of the Electronic Ground State in Six-Coordinate Copper(II) Complexes. *Angew. Chem. Int. Ed.* **1998**, *37*, 2221–2223.